A 3-RSR Haptic Wearable Device for Rendering Fingertip Contact Forces

Daniele Leonardis, *Member, IEEE*, Massimiliano Solazzi, *Member, IEEE*, Ilaria Bortone, *Student Member, IEEE*, and Antonio Frisoli, *Member, IEEE*

Abstract—A novel wearable haptic device for modulating contact forces at the fingertip is presented. Rendering of forces by skin deformation in three degrees of freedom (DoF), with contact—no contact capabilities, was implemented through rigid parallel kinematics. The novel asymmetrical three revolute-spherical-revolute (3-RSR) configuration allowed compact dimensions with minimum encumbrance of the hand workspace. The device was designed to render constant to low frequency deformation of the fingerpad in three DoF, combining light weight with relatively high output forces. A differential method for solving the non-trivial inverse kinematics is proposed and implemented in real time for controlling the device. The first experimental activity evaluated discrimination of different fingerpad stretch directions in a group of five subjects. The second experiment, enrolling 19 subjects, evaluated cutaneous feedback provided in a virtual pick-and-place manipulation task. Stiffness of the fingerpad plus device was measured and used to calibrate the physics of the virtual environment. The third experiment with 10 subjects evaluated interaction forces in a virtual lift-and-hold task. Although with different performance in the two manipulation experiments, overall results show that participants better controlled interaction forces when the cutaneous feedback was active, with significant differences between the visual and visuo-haptic experimental conditions.

Index Terms—Haptic, wearable, fingertip, cutaneous, tactile, force, feedback, RSR

1 Introduction

Haptic devices introduce sense of touch for interaction in virtual environments and teleoperation applications. Although most haptic devices rely on kinesthetic feedback provided to the user, other devices make use of tactile stimulation, vibrotactile or electro-tactile stimulation [1]. Also cutaneous feedback plays a relevant role in haptic perception due to the richness of mechanoreceptors in fingerpads [2]. Recent studies have shown how cutaneous stimuli are fundamental in recognizing shapes [3], in discrimination of curvature [4], [5], [6] and local surface orientation [7], in improving the illusion of presence in virtual and remote environments [8], [9], [10].

Wearable cutaneous displays exploit the above mechanisms to induce local skin deformation at the fingerpad simulating the contact interaction with a virtual object. Different physical cues during fingerpad interaction with objects are responsible for the sensory stimulation of mechanoreceptors, among which an important role is due to change in contact surface [11], local surface orientation [6] and skin stretch [12]. For the reasons above, a variety of different cutaneous interfaces have been devised relying on different principles of eliciting cutaneous deformation at fingerpad, see Fig. 1.

A class of cutaneous devices exploit the change of contact location. This aspect was originally approached in [13] with a non wearable solution. More recently [14] presented a wearable haptic device with five-bar linkage mechanism for rendering two-DoF force feedback at the fingerpad: the reduction of movement to the planar case brought to significant advantages in terms of weight and bulk, but imposed strong limitations in terms of perceived feedback.

Another mean to achieve cutaneous deformation is the display of contact status and orientation through a moving contact surface. In order to improve cutaneous information with contact geometry information, a first cutaneous device was developed by Frisoli et al. in [15] and then simplified in a dual finger configuration in [16], where a voice coil actuator was used to provide high speed dynamics of contact. Another simpler design was presented in [17], where simulation of tangential frictional force was limited to one-DoF only. Similarly Pratticchizzo et al. [18] introduced a three-dof wearable device for cutaneous feedback based on a parallel architecture and tendon based actuation.

Skin stretch is another mechanism of local skin deformation employed to elicit force response. In [12], a simple haptic device was realized to accurately guide users through planar hand movements; more recently in [19] a three-DoF skin stretch display was put inside the handle of a 1 point kinaesthetic haptic interface. It was demonstrated that increasing speed beyond 1 mm/s the communication of stimuli did not result in significant improvement [20] Provancher et al. [21] conducted experiments in support of the hypothesis that the addition of skin stretch to kinesthetic resistance forces increases the perceived friction magnitude. Previous results yielded difference thresholds with percent changes that ranged from 0.28 to 0.19 across friction levels, μ_s = 0.2-0.8, respectively. The same authors found that a small amount of skin stretch (0.27 mm) superimposed on

• *The authors are with the Perceptual Robotics Laboratory, TeCIP Institute, Scuola Superiore Sant'Anna, Pisa PI 56127, Italy. E-mail: {d.leonardis, m.solazzi, i.bortone, a.frisoli}@sssup.it.*

Manuscript received 29 July 2016; revised 18 Nov. 2016; accepted 5 Dec. 2016. Date of publication 15 Dec. 2016; date of current version 14 Sept. 2017. Recommended for acceptance by M. Santello.
For information on obtaining reprints of this article, please send e-mail to: reprints@ieee.org, and reference the Digital Object Identifier below.
Digital Object Identifier no. 10.1109/TOH.2016.2640291

(a) ref. [13] (b) ref. [14] (c) ref. [15]

Fig. 1. Recent cutaneous devices developed in literature.

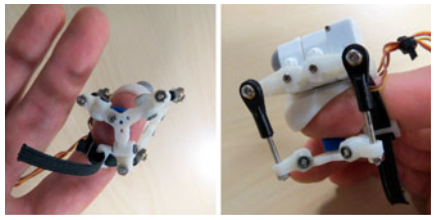

(a) Worn on index finger (b) Side view

Fig. 2. The proposed device for rendering skin stretch at the fingertip.

kinesthetic resistance can have a significant effect on perceived friction [21]. It becomes clear the need to identify the design parameters required by a cutaneous interface in order to be small and portable [18]. For instance size, weight and power consumption can be minimized by lowering stimulus speed and displacement requirements.

In particular, when manipulation is concerned, neurophysiological studies have already shown the role of both grip and loading forces [2], highlighting the selective response of SAII and FAI afferents to loading/unloading forces[22], justifying the need of rendering up to the 3dof forces at fingerpad during manipulation. Moreover the benefit of a three-DoF skin deformation haptic feedback versus one DoF and no feedback conditions has been already demonstrated in [19]. Based on the above, we devised the design of a novel wearable fingertip device capable of displaying both interaction forces by skin deformation in three-DoF and contact—no contact transition. The device (Fig. 2) has been conceived based on an hybrid approach: it displays change in contact surface by means of the displacement of a tactor, and once in contact it exploits three dimensional skin stretch deformation of the fingerpad to display forces.

A specific asymmetric three-RSR kinematic design was developed for minimizing encumbrance within the hand workspace and mechanical interference with other fingers. It resulted in a highly wearable device with compact dimensions and light weight, particularly suitable for rendering haptic feedback during manipulation in virtual environments.

The device is presented in Section 2, with details of the kinematics and of the method applied for solving in real-time the differential inverse kinematic. Three experiments were carried out to evaluate the effectiveness of the cutaneous feedback rendered by the proposed device. The first experiment regards discrimination of directional deformation of the fingerpad and is presented in Section 3. The second and third experiment involve virtual manipulation in an unconstrained pick-and-place task (Section 4) and in a controlled lift-and-hold task (Section 5) respectively. Results and discussion are presented within specific Sections of each experiment; general conclusion are presented in Section 6.

2 The Fingertip Wearable Haptic Device

In this work, we propose a novel wearable haptic device . The rigid parallel kinematic design (Fig. 2) was conceived for moving the skin tactor (6 mm diameter, silicon) in three-DoF, with the capability of rendering contact and no-contact conditions. By means of the parallel structure, all the actuators were mounted on the base fixed to the back of the fingertip. Thus, the encumbrance within the hand workspace was minimized to the only end-effector with the skin tactor. Moreover, in order to reduce dimensions and inter finger interference, rotary actuators were mounted with parallel axes, orthogonal to the finger length, and the first moving links of each actuator were aligned on planes parallel to the moving plane of the finger phalanxes. This minimized mechanical interferences of the device with the finger itself, with other fingers and with other devices worn on the other fingers.

With respect to the initial prototype presented in our preliminary work [23], wearability of the device has been further improved by means of even more compact servo actuators and an optimized plastic frame. In the new design, the aspect ratio and the mass of components displaced at the back of the finger was reduced to the minimum: the center of mass of the whole device resulted closer to the middle of the finger, thus improving stability. The shape of the rigid plastic thimble was designed in order to fix just to the nail and the very end of the fingertip, with the purpose of accomodating a wider range of finger sizes. Furthermore, rigidity of the rotary joints was improved through a steel shaft supported by bushings at both ends. Final dimensions of the device were $18 \times 32 \times 32$ mm (excluding the moving platform beneath the fingerpad), with a mass of 16 g, including actuators and the moving platform. Such design resulted into a three-RSR asymmetric parallel kinematics of the device (Fig. 3a), and led to the development of the non-trivial solution for the inverse kinematics presented in Section 2.1.

The device was designed for rendering constant to low frequency deformation of the fingerpad in three DoF, combining light weight with relatively high output forces. Electromagnetic RC servo motors were implemented for actuating the device (HK-282A RC servo motors, maximum torque 0.2 Nm), due to the unmatched low mass and compact size (2 g $16 \times 18 \times 8$ mm each), including gear reduction and embedded absolute position sensing and control. The presence of gear reduction allowed high force-to-weight ratio, but limited the output bandwidth (below 50 Hz according to the off-the-shelf position control of the servomotors), thus preventing the haptic device from rendering fast transients. Yet, it is worth to note that since the device is grounded on the fingertip itself, high frequency of the control loop (1 Khz is a common value for kinaesthetic haptic devices) is not required here for ensuring stability of the force feedback. Furthermore, other modules of the integrated system, i.e., the optical position tracking and physical simulation in the VR, impose limits to the bandwidth of the system comparable to those of the actuators. The use of RC servomotors derived from a nowadays long-term optimization of this technology in the radio-controlled models field, whereas low-mass and dimensions are features still unmatched by servomotors designed for other applications, even with higher quality and cost of components.

The three servo motors were driven through a Pololu Micro Maestro control board. Each actuator was equipped with an embedded position control (maximum angular velocity $500°/s$, accuracy $\approx 1°$, 50 Hz refresh rate of the angular

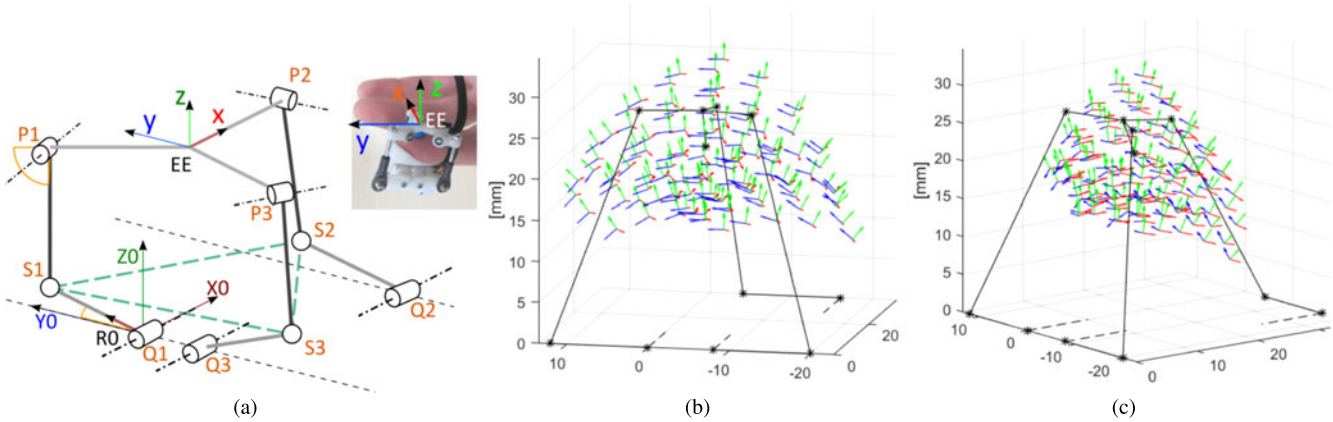

Fig. 3. (a) Kinematics of the haptic device, and representation of the end effector system of reference superimposed to the real device. Q1, Q2, and Q3 are the actuated rotary joints, EE is the skin tactor. (b) and (c) Workspace of the end-effector, obtained considering a 45° angular displacement range for Q1, Q2, and Q3.

position reference). The maximum linear forces that can be exerted by the skin tactor with position centered in the middle of the workspace are: 2.42, 2.73 and 4.16 along the distal, radial and normal axes of the fingerpad respectively (values are theoretically computed through kinematics of the device and considering maximum output torque of the actuators).

2.1 Kinematics

The three-RSR mechanism presents a combined motion of the end effector, so that variation of the joint angles results in variation of both position and orientation of the end effector.

2.1.1 *Differential Kinematics*

The motion of the end effector can be better described by the analysis of the constraint and actuation wrenches for each leg of the mechanism [24]. By screw theory [25] for each joint of a leg the twist $\$_{i,j}$ is associated, using Plücker coordinates and considering the origin of the base system as the pole for representation of screws; j denotes the number of the joint and i the number of the leg. The spherical joint has been modeled as three revolute joints with incident axes. All the twists of a leg can be arranged in the system of twists $\$_i$

$$\$_i = \begin{pmatrix} \$_{i,1} & \$_{i,2} & \$_{i,3} & \$_{i,4} & \$_{i,5} \end{pmatrix}. \tag{1}$$

The constraint wrench of the leg $\mathbf{W}_{c,i}$ is then calculated as the reciprocal of the system $\$_i$, so that

$$\mathbf{W}_{c,i} \otimes \$_{i,j} = 0 \qquad \text{for} \qquad j = 1, \ldots, 5, \tag{2}$$

where $\otimes$ denotes the product of reciprocity between screws.

Analogously the actuation wrench of the leg $\mathbf{W}_{a,i}$ is calculated as the wrench reciprocal to the leg twists except the twist associated to the actuated joint

$$\begin{cases} \mathbf{W}_{a,i} \otimes \$_{i,j} = 0 & \text{for} \quad j = 1, \ldots, 5, \quad j \neq 1 \\ \mathbf{W}_{a,i} \otimes \$_{i,j} \neq 0 & \text{for} \quad j = 1 \end{cases} \tag{3}$$

with the actuation at the first joint.

For the three-RSR mechanism, according to Equation (2), the constraint wrenches are zero pitch screws always passing through the center of the spherical joint, as represented in Fig. 4. The direction of each wrench $\mathbf{W}_{c,i}$ can be geometrically found as the intersection between the plane identified by the axes of the first joint $J_{i,1}$ of the leg and the center of the spherical joint and the plane identified by the axes of the last joint $J_{i,5}$ of the leg and the center of the spherical joint. For the general case of skew $J_{i,1}$ and $J_{i,5}$ axes, the wrench $\mathbf{W}_{c,i}$ intersect the two axes in two different points, for example P_1 and P_2 for the first leg in Fig. 4. The constraint wrenches $\mathbf{W}_{c,i}$ form a system of three skew forces, whose linear combination lie on the regulus of an hyperboloid, so the allowed resultant motion of the end effector can be described as the composition of three rotations around skew axes.

Given the constraint wrenches $\mathbf{W}_{c,i}$, the constraint Jacobian can be defined as a 6 by 3 matrix

$$J_c = \begin{pmatrix} \mathbf{W}_{c,1} & \mathbf{W}_{c,2} & \mathbf{W}_{c,3} \end{pmatrix}. \tag{4}$$

By definition given any feasible motion of the end effector $\$_{EE}$ the following equation holds:

$$J_c^T \otimes \$_{EE} = 0. \tag{5}$$

Dividing the motion of the end effector in translational and rotational velocity, and the constraint Jacobian in forces and torques as

$$J_c = \begin{pmatrix} J_{cF} \\ J_{cT} \end{pmatrix} \qquad \$_{EE} = \begin{pmatrix} \omega \\ \mathbf{v} \end{pmatrix}. \tag{6}$$

Equation (5) can be written as

$$J_{cF}^T \mathbf{v} + J_{cT}^T \omega = 0. \tag{7}$$

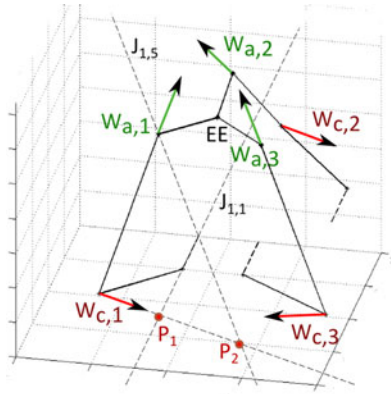

Fig. 4. Constraint and actuation wrenches of the mechanism.

Solving Equation (7), if J_{cT} is invertible, the relation between translational and rotational velocity is defined

$$\boldsymbol{\omega} = (-J_{cT}^{-T} J_{cT}^{T})\mathbf{v} = J_m \mathbf{v}. \quad (8)$$

Equation (8) represents the necessary rotation of the end effector according to the desired translation.

2.1.2 Direct and Inverse Kinematics

Since the aim of our device is rendering of forces on the fingertip by skin deformation, and the shape of the tactor is not designed to apply torques, we focused on the control of the translations of the end effector only. Unfortunately solving both the direct and inverse kinematics of the device presents several issues. The direct kinematic problem of the three-RSR mechanism, except for particular cases with axial symmetry and equal lengths for all the links [26], does not present a unique analytical solution; it has been demonstrated that given any joint angles $\mathbf{q} = [\theta_1, \theta_2, \theta_3]$ there exist four real solutions obtained by a 16th order polynomial [27].

The feasible poses of the mechanism were so determined through a computational approach. Given the generic pose of the end effector $\mathbf{p} = [\mathbf{x}(x, y, z), R(\phi, \theta, \psi)]$, where $\mathbf{x}$ and R represent respectively the Cartesian position and the rotation matrix associated to the Euler's angles ϕ, θ, ψ, a system of three nonlinear equation represents the constraint for the six coordinates [28], and can be numerically solved to compute the desired joint angles $\mathbf{q}$. Since the computational cost of the numerical solution of the 16th order polynomial is high, a numerical iterative algorithm for solving the direct kinematics problem was developed on purpose.

By splitting the mechanism in two halves, the position of the vertexes of the triangle $S_1S_2S_3$ can be computed though two independent kinematic chains: one from the side of the actuators through joints Q_i and one from the side of the moving platform through the joints P_i. Once the joint angles q_i are given, the triangle $S_1S_2S_3$ is univocally through the first kinematic chain. Then positions of joints S_i can be derived through the second kinematic chain as a function of the unknown angles of joints P_i. By imposing so the geometric constraint of same distance of points S_i, derived through the two different kinematic chains, a set of three non linear equations is derived, whose solution can be numerically found through an iterative procedure, and so the values of unknown P_i joint angles are determined.

2.1.3 Trajectory Generation Algorithm: Implementation and Validation

Relation (8) can be implemented in discrete form at time step i

$$\boldsymbol{\omega_i} = J_m(\mathbf{x_i})\mathbf{v_i}. \quad (9)$$

Given a desired reference position $\mathbf{x_i}$ of the end effector at time step i, the corresponding end-effector orientation, expressed by the rotation matrix R_i, can be computed numerically as

$$\begin{cases} \mathbf{x}_i = \mathbf{x}_{i-1} + \mathbf{v_i}\Delta t \\ R_i = R_{i-1} + \Omega_i(\boldsymbol{\omega_i})R_{i-1}\Delta t, \end{cases} \quad (10)$$

where Ω_i is the skew-symmetric matrix associated to the angular velocity vector $\boldsymbol{\omega_i}$ at time i.

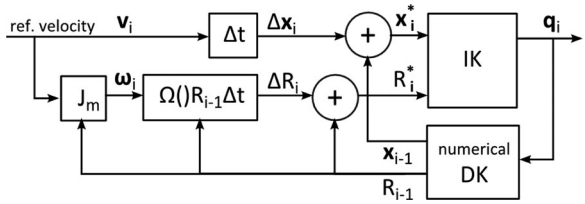

Fig. 5. Scheme of the implemented algorithm solving the inverse kinematics: $\mathbf{x}_i^*$ and $\mathbf{R}_i^*$ indicate position and rotation matrix of the end effector at time step i before drift correction through computation of the direct kinematics.

The desired angular positions at time step i of the actuators $\mathbf{q_i}$ are then computed through the analytical solution of the inverse kinematics, given the current pose $\mathbf{x_i}$ and orientation R_i of the end effector.

However, the discrete integration of (9) introduces numerical errors that might be accumulated and might be propagated to the computation of J_m. In order to limit the computational drift, a closed-loop correction mechanism was introduced, as summarized in the scheme of Fig. 5. Based on the actual joint reference angles $\mathbf{q_i}$, one iteration of the numerical solution of the direct kinematics is computed, and resulting values are used to update the position and orientation of the end effector, that will be used in the next step of computation.

To enhance convergence and minimize numerical errors, the reference velocity of the end-effector was limited to 30 mm/s. Such value is comparable with the maximum velocity at the end-effector that can be obtained with the implemented actuators. Execution time for one iteration of the algorithm was about 80 microseconds on a Pentium i3, 3.30 GHz, 64 bit PC. Considering the limited bandwidth of the servomotors and the sample rate imposed by other modules of the system integrated with VR (optical tracking and physics simulation executing at 100 Hz) the execution frequency of the inverse-kinematics algorithm was set to 100 Hz. Fig. 6 shows performance of the algorithm for a reference movement, starting from the middle position of the workspace and directed toward the limit of the workspace at the maximum permitted linear velocity. Good performance in convergence of the algorithm was obtained, with the maximum absolute error of 0.33 mm.

The inverse kinematics algorithm and the precision of the device itself was evaluated by measuring position error of the end effector through an optical tracking system (Optitrack, V120 Trio). Relative position error of the tracking system itself was evaluated in the area proximal to the workspace of the device, by measuring distance of two markers fixed onto a moving rigid body. Error of the optical tracking system was estimated below 0.1 mm. A set of points uniformly distributed along the three orthogonal axes of the workspace (step 1 mm, limits ± 4 mm from the origin) was given as position reference to the device. The obtained mean error was 0.202 ± 0.098 mm, while the maximum error was 0.43 mm.

3 Direction Discrimination Experiment

The first perception experiment focused on the discrimination of skin stretch direction. The experiment evaluated subjects' capability of identifying different directions of tangential skin deformation at the fingertip, provided by the developed haptic device. This preliminary experiment

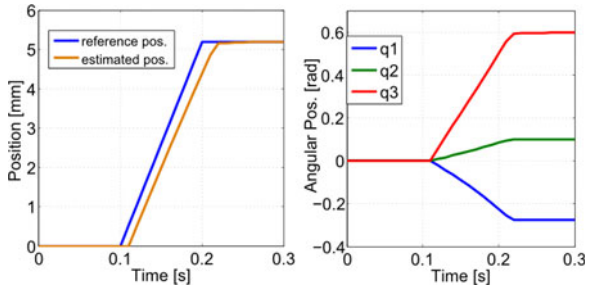

Fig. 6. Convergence of the implemented algorithm for solving the inverse kinematics in real time. Left figure shows the reference position (ramp with velocity equal to 30 mm/s) and position estimated in real time by executing the algorithm at 100 Hz. Right figure shows the real time computed angular position reference sent to actuators.

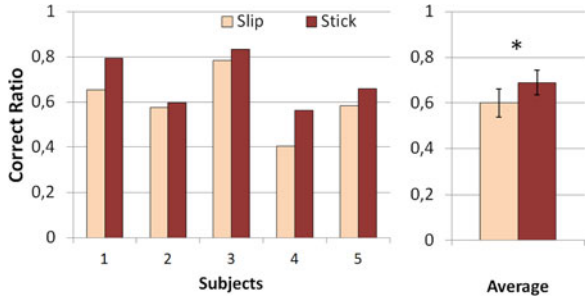

Fig. 7. Barplot representing the correct ratio for each subject for the Stick and Slip conditions, respectively, and the grand average over the subjects.

evaluated whether the provided haptic feedback was consistent during both stick and slip conditions of the skin tactor, and was performed before moving to more complex manipulation experiments presented in the following sections, where tangential deformation is mixed with normal components generated by grasping of virtual objects. The experiment was structured as a forced-choice paradigm with stimuli consisting in deformation of the fingerpad along eight different directions on the tangential plane, with a fixed offset for normal indentation. Stimuli belonged to two different classes, differing for the stick or slip condition of the tactor moving on the fingerpad.

3.1 Procedure and Methods

Five subjects participated in the experiment (27-35 years old, one female, four males, all right-handed), providing written consent to participate. Subjects seated on a chair in front of a desk with a computer screen. The haptic device was worn at their right index finger, with the hand leaning on a soft support. Stimuli consisted of deformation of the fingertip along eight different directions on the tangential plane, corresponding to the four cardinal directions plus the four intermediate diagonals (Fig. 10). Radial displacement of the tactor with respect to the starting position was 1 mm for all stimuli. With respect to the applied normal indentation, two different classes of stimuli were set, referred hereafter as "Stick" and "Slip" classes. Stimuli of the Slip class were calibrated with a lower offset indentation (0.5 mm over the contact threshold), resulting in slippage of the skin tactor during the tangential displacement. Conversely stimuli of the Stick class applied a higher offset indentation (2 mm over the contact threshold), in order to obtain radial deformation of the fingerpad without slip. The offset indentation value was experimentally determined in order to obtain the intended stick and slip conditions for all the subjects. At the beginning of the experimental session, the offset of the skin tactor was set in order to be centered with respect to the fingerpad. Once the contact threshold of the tactor was calibrated for each subject, stimuli of both classes were presented one by one to the subject, for a total of 16 stimuli (eight directions for both the Slip and Stick classes). Each presentation of the stimulus consisted of three steps: first, the tactor moved in contact with the fingerpad at the reference offset indentation. After 2 s, the tactor moved 1 mm along the reference tangential direction. After 2 s, the tactor moved out of contact from the fingerpad. After the preliminary presentation of the set of stimuli, a random sequence of stimuli was presented to each subject, belonging to both the Stick and Slip classes in random order. After presentation of each stimulus, subjects had to mark the perceived tangential direction among the set of eight possible choices. The answer was given through a graphic user interface displayed on a monitor in front of the subject. A sequence of 96 stimuli was presented to each subject, obtaining a total of 480 trials.

3.2 Results and Discussion

Answers collected in the experiment were divided between the Stick and Slip classes of stimuli. The bargraph in Fig. 7 shows correct ratio values of each subject for the Stick and Slip conditions respectively, and the grand average over the subjects. The obtained average correct ratio was relatively high if compared to the chance value of 0.125 related to the proposed forced-choice paradigm, and equal to 0.60 for the Slip and 0.69 for the Stick condition respectively. Though computed with a limited number of subjects, difference between correct ratio of the two experimental conditions was significant (paired t-test, $p < 0.027$), and all the subjects reported higher discrimination performance for the Stick condition than for the Slip condition. This result might be expected since in the Stick condition deformation of the fingerpad and forces exerted by the tactor in direction of the cue are higher, yet it has to be noted that the slip phase occurring in the slip condition might introduce an additional, transient cutaneous perception informative of the direction of the cue. Furthermore, different normal indentation for the two conditions introduced a different offset deformation of the fingerpad that could have influenced the perception of the stimuli.

Regarding the device operation, though capability of sensing the stick and slip phases could be interesting for a more sophisticated cutaneous feedback, the experiment assessed that all the subjects were capable of discriminating direction of the cutaneous cues with relatively high accuracy in both Stick and Slip conditions. Fig. 8 shows confusion matrices of the Slip and Stick conditions. Numerical values reported in each cell represent the occurrence of a specific answer (horizontal axis) in response to a specific stimulus (vertical axis), normalized by the total number of presentations of the stimulus. Cells on the diagonal of the confusion matrix represent the correct ratio obtained for each stimulus. All directions, except SW, were discriminated with similar accuracy (max 0.85, min 0.67 for the Stick condition, max 0.69, min 0.59 for the Slip condition), with incorrect answers concentrated on cells corresponding to the neighboring directions of the stimulus. SE stimulus was discriminated with a noticeable worse performance (0.36 for the Stick condition and 0.46 for the Slip condition). The

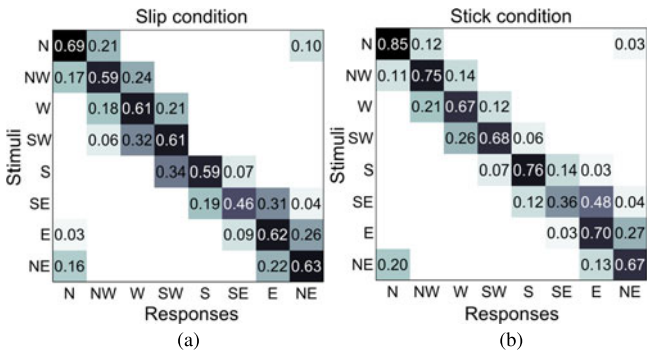

Fig. 8. Confusion matrices representing occurrence of answers (horizontal axis) assigned to each stimulus of the Slip (top) and Stick condition (bottom).

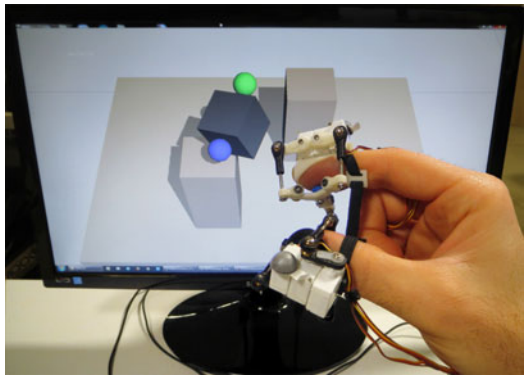

Fig. 9. Experimental setup: The computer screen, the position tracking system, and the wearable haptic devices for thumb and index fingers.

result might be addressed to dishomogeneity in the workspace of the device: the experimental session in Section 4.1.2, introducing a force sensor for measuring interaction forces of the device with the fingerpad, shows that forces exerted along the SW direction were less accurate with respect to those along other directions.

It is interesting to compare overall results to those obtained in [29], where perception of directional skin deformation of the fingerpad was evaluated with a dedicated experimental setup. In the study, subject reported no errors in identifying 1 mm fingerpad skin displacement, however due to the specific experimental design, discrimination was performed along the four cardinal directions. In the study we present, introduction of diagonal directions lowered the discrimination accuracy. Considering diagonal directions, results reported in [12] show higher accuracy of subjects in discriminating stretch directions of the fingerpad within a similar experimental setup. The difference might be explained by different characteristics of the haptic device used in [12]: in particular, the device was not wearable and mounted a fixed ring around the tactor, this probably allowed a more stable fixing between the finger and the body of the device, with higher interaction forces and amplification of the relative skin stretch of the fingerpad.

4 Pick and Place Manipulation Experiment under Ecological Conditions

It has been shown that healthy individuals can accurately control their grasping forces in manipulation tasks, such as lifting an object, using information obtained from mechanoreceptors in the fingertips [2]. In particular, it has been shown that in the natural execution of a grasping task, grasping forces are held just above the level of static friction required to avoid slippage [30], while in case sensory feedback is limited, such as in virtual environments, the safety margin in terms of forces required to grasp and lift an object is increased [31].

Effectiveness of sensory information provided by the proposed device was investigated through an experiment involving fine manipulation of virtual objects presented in ecological conditions. The proposed task was not a perception task, focused on a specific sensory modality, but a pick and place task where the subjects were free to adopt more comfortable strategies for accomplishing the task. The goal of the experiment was to investigate whether the addition of cutaneous feedback to visual feedback was sufficient to improve grasping performance in a virtual manipulation scenario. According to our scientific hypothesis, we expected that the addition of cutaneous feedback will improve grasp performance, measurable in terms of reduction of the grasp normal force necessary to lift the virtual object. Due to the role played by vision in the anticipatory movement of grasp, e.g., finger pre-shaping for grasping according to the size of the object, and the inability of the device in rendering the slip condition, we did not expect to see significant variations in terms of task result (i.e., percentage of box fallen or crushed). The experiment compared task performance in terms of virtual interaction forces, task results, and questionnaire.

4.1 Procedures and Methods

Subjects sat in front of a monitor and wore two haptic devices, one at the right index and one at the thumb. An optical tracking system was used (OptiTrack V120 Trio, Motive, USA) for tracking position and orientation of the fingertip haptic devices (Fig. 9).

A computer graphic representation of a virtual cube (40 mm size), a table and two static platforms were introduced in the virtual scene. Index and thumb fingertips were represented by two spherical objects with 10 mm diameter, coloured green and blue respectively. The point of view was coherent with the body pose of the participant. The virtual scenario and real-time rendering were developed with XVR framework (eXtreme Virtual Reality [32]). Physics simulation of interaction forces generated by gravity, friction, stiffness and collisions was performed using PhysX by NVIDIA. The physics engine was updated with the external position references of the tracked fingers at 120 Hz, although additional convergence loops might be autonomously executed by the engine at run-time. The virtual coupling between the position of the tracked fingers and the virtual fingertips simulated by the physics engine was implemented by using the specific stiffness coefficient measured for each subject in the previous experimental session (Section 4.1.2)

During the experiment, subjects were asked to pick and place the virtual cube between two fixed platforms displayed in the virtual scenario. Each trial could terminate with three different results:

- Completed: the cube was correctly picked from the starting platform and placed over the target platform.
- Dropped: the cube was moved and dropped aside the target platform.

- Broken: the cube was grasped with a peak force exceeding a fixed threshold value representing the breaking force threshold of the cube.

4.1.1 Experimental Design

Fifteen subjects (age 25-42, two female) were enrolled to the experiment, providing written consent to participate. All but one were right handed and did not present any dysfunction of the fingers. The experiment was based on a within subjects repeated-measurements 2×2 factor design. The first factor was the sensory feedback provided to the subjects during the manipulation:

- Cutaneous plus Visual feedback (CV condition): visual feedback of the virtual environment was provided through a monitor, and cutaneous devices rendered virtual interaction forces at the fingertips.
- Visual feedback (V condition): only visual feedback of the virtual environment was provided, while fingertip haptic devices were turned off.

The order of the V and CV sessions was balanced among subjects in order to minimize biases due to either training effects or fatigue effects. Before each session, subjects practiced a few task repetitions, then a sequence of 50 trials was performed. Subjects had no limits in time to accomplish the task.

The second factor was the weight of the cube that the subjects grasp.

- Heavy cube: mass 40 g, breaking force 1.8 N, friction coefficient: static 0.55, dynamic 0.5.
- Light cube: mass 20 g, breaking force 1.25 N, friction coefficient: static 0.55, dynamic 0.5.

The two cubes of different weight were presented in random order. Colour of the heavy cube was black while the light cube was coloured white, yet subjects were not told about different physical characteristics of the cubes. With the given parameters of mass, friction and gravity of the physical simulation, the minimum grasping force (modulus of the tangential plus normal components) required to lift the cubes was estimated as 0.41 and 0.20 N for the heavy and light cube respectively.

Before proceeding with the experimental setup of the virtual manipulation scenario, a preliminary experimental session was performed in order to characterize for each participant, by means of a force sensor, the stiffness of the fingerpad plus the haptic device. The stiffness coefficient measured for each subject was used to convert interaction forces between the fingertips and the virtual environment in displacement coordinates for the skin tactor of haptic devices.

Once the haptic devices were worn on the thumb and index fingers, the position of each skin tactor was tuned by the experimenter in quasi-contact condition with the fingerpad. During device operation, reference displacement of each skin tactor was computed within the XVR virtual environment and sent to a Matlab Simulink model solving in real time the inverse kinematics. Obtained angular positions were transmitted through USB to the embedded position control loop of the actuators at 50 Hz sample rate (standard frequency of the rc analog micro-servo actuators).

At the end of each session, an evaluation questionnaire based on a seven-points Likert scale was proposed to the subjects. The questionnaire was composed of a set of control questions ("Control" group), a set of questions about the overall virtual experience ("Virtual Experience" group),

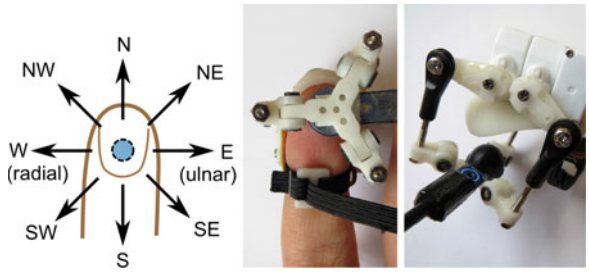

(a) Stretch directions (top view) (b) Device with force sensor (bottom view) (c) Side view

Fig. 10. Experimental setup with force sensor implemented for the direction discrimination experiment, and for calibration of the system on subject specific stiffness of the fingerpad.

and a set of specific questions assessing issues related to the overall manipulation experience and specific physical characteristics of the presented cubes ("Manipulation" group). Some items related to experience and multisensory engagement were based on the original Witmer and Singer's presence questionnaire [33]. The questionnaire group and questions are presented in Table 2.

4.1.2 Individual-Based Characterization of the Force-Indentation Response

Before conducting the experiment, an experimental procedure was conducted for each subject to characterize the individual-based force-indentation response. One fingertip haptic device was equipped with a force sensor in place of the skin tactor (Fig. 10) in order to measure interaction forces between the device and the fingerpad. The force sensor was an OptoForce OMD-10-SE-10N (three axes, range 10 N, resolution 1 mN), an optical force sensor particularly suitable for the purpose of the experiment due to its compact dimensions (10 mm diameter silicon rubber hemisphere).

Subjects wore the haptic device at the right index finger and were instructed to hold their hand as still as possible during the experiment. The force sensor was placed in contact with the fingerpad of the subject with 1 mm indentation. Then, the haptic device was driven with a pre-defined movement sequence applying 1.5 mm skin deformation along nine directions: eight directions on the tangential plane, as shown in Fig. 10 and similar to Section 3, plus one normal direction. Finger deformation was applied at 1 mm/s linear velocity, and force sensor data was acquired at 100 Hz. Between two subsequent displacements, the sensor was moved out of contact and then again in contact with the fingerpad along the normal direction. The measuring procedure was automatically repeated three times for each direction of displacement.

At the displacement and velocity used in this experiment, the force-displacement curve was observed to be nearly linear. After discarding those data affected by eventual slip of the sensor with the skin, a linear regression was fit to each test displacement.

Data measured in all tangential and normal directions are shown for one representative subject in the three dimensional plot of Fig. 11b. Axes of the plot represent the axes of the three DoF force sensor in contact with the fingerpad. Graphs in Fig. 11c show for each direction of displacement the force-displacement curve along with fit lines measured during one repetition for eight representative subjects. The

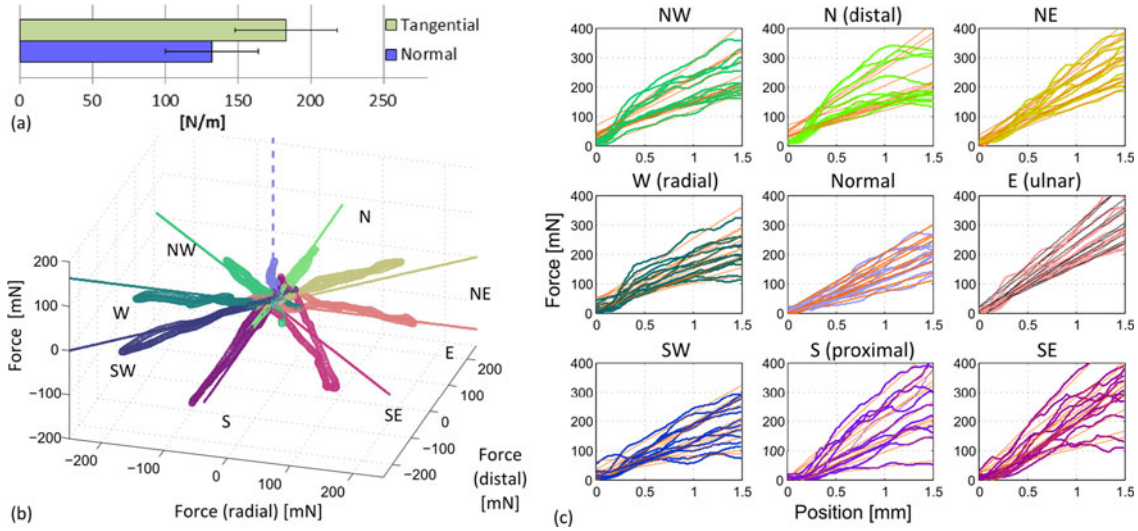

Fig. 11. Measured force corresponding to a normal indentation and lateral stretch of 1.5 mm. Figure (a): mean stiffness coefficient computed for normal and tangential directions. Figure (b): Three DoF force measurement in cartesian space for one representative subject. Figure (c): force-displacement characteristic for each direction and for each subject. Orange lines represent the linear fit for each subject.

values of the average fingerpad stiffness, to be used in the virtual environment, were computed for each subject by averaging slope of the fit lines over the three measurement repetitions and over the eight tangential directions. Grand average over the subjects of the obtained stiffness value was 132 ± 30 N/m for the normal direction and 183 ± 35 N/m for the tangential direction (barplot in Fig. 11a, with average coefficient of determination of the linear fit (R-squared) equal to 0.952 and 0.921 for the normal and tangential directions respectively. Values of the measured stiffness appear noticeably different with respect to literature (i.e., the work presented in [20], [34]). Since here the purpose of the measurement was solely to calibrate the cutaneous feedback provided to each subject, the structure of the device itself and its fixing to the fingertip were included in the measurement of stiffness, thus highly reducing the measured value if compared to the fingerpad stiffness only.

4.1.3 Data Analysis

Interaction forces between the cube and virtual fingers were recorded throughout the experiment and averaged for each trial. In the averaged results, only data recorded while the cube was grasped and lifted were considered, with the purpose of eliminating eventual force peaks generated by combined collision between fingers, cube and the static platform. In the analysis the Mean Force is computed averaging over trials the mean absolute interaction force between fingers and cube measured during each trial. The Peak Force is computed averaging over trials the peak force measured during each trial. A within-subjects repeated measurements ANOVA was conducted, followed by analysis of interaction among factor, main effects (LSD post-hoc corrections). Analysis of simple effects was performed only for items presenting significant difference. Non parametric tests were used for analysis of questionnaire results. All data were processed using Matlab, statistics was performed via IBM SPSS vers.19.

4.2 Results and Discussion

In the presented experiment we expected that, whereas cutaneous feedback device could effectively render coherent information of fingertip interaction (CV condition), average grasping forces would be lower in CV than in the V condition, and closer to the minimum required threshold for completing the task.

Averaged results of the statistical analysis is reported in Table 1. As expected, the CV condition providing both visual and cutaneous feedback presented a lower grasping force than V with visual feedback only (V: 0.83 N, CV: 0.75 N, $p < 0.04$); significantly higher force was applied to lift up the heavier object (Heavy: 0.86 N, Light: 0.72 N, $p < 10^{-8}$), while no significant interaction was present between the two factors. This was more evident in the analysis of data of maximum exerted peak force within each trial, with lower values in the CV condition (V: 0.94 N, CV: 0.86 N, $p < 0.04$), and higher peak force for the heavy object (Heavy: 0.99 N, Light: 0.81 N, $p < 10^{-8}$).

TABLE 1
Statistics of within-Subjects ANOVA, * $p < 0.05$, **$p < 0.01$

Factor	Item	V	CV	Statistics	p value
Feedback	*Mean force*	0.83 ± 0.06 N	0.75 ± 0.06 N	F(1,18) = 5	$p < 0.04$ **
Condition	*Peak force*	0.94 ± 0.07 N	0.86 ± 0.07 N	F(1,18) = 5	$p < 0.04$ **
		Light	Heavy	Statistics	p value
	Mean force	0.72 ± 0.06 N	0.86 ± 0.06 N	F(1,18) = 118.15	$p < 10^{-8}$ **
Weight	*Peak force*	0.81 ± 0.06 N	0.99 ± 0.07 N	F(1,18) = 118.15	$p < 10^{-8}$ **
Condition	*Mean force*			F(1,18) = 1.24	NS
* Weight	*Peak force*			F(1,18) = 1.54	NS

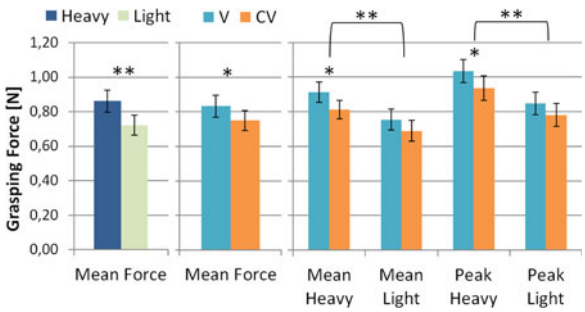

Fig. 12. Average and peak grasping forces averaged for all the subjects in the V and CV conditions.

Barplots in Fig. 12 presents the average interaction forces separately for the Heavy and Light virtual cubes in the V and CV feedback conditions. Interaction forces in V are generally higher than in CV, for both light and heavy cubes: when the haptic feedback was presented both the Mean Force and Peak Force are lower. A significant difference between the two conditions has been observed with heavy cubes both for the Mean Force (V: 0.91 N, CV: 0.81 N, $p < 0.010$ paired t-test) and for the Peak Force (V: 1.04 N, CV: 0.94 N, $p < 0.023$ paired t-test). Though results show the manipulation task could be performed with comparable performance with visuo-haptic or visual feedback alone, presentation of cutaneous feedback provided more consistent sensory information, inducing a more natural behavior with lower average grasping force. In particular results suggest the cutaneous feedback was more effective for the heavy object, moreover, data show that average forces were closer to the minimum required threshold for the heavy cube (0.81 N versus the minimum force of 0.41 N) than for the light cube (0.69 N versus the minimum force of 0.20 N). This might suggest the experimental setup was more accurate in reproducing contact forces comparable to the weight of the heavy cubes, while for lower forces, closer to the contact-no contact threshold, the precision of the tracking system, of the physical engine running in real-time and of the device control begins to present some limits. Subjects showed to be able to complete the task even in the visual condition with good accuracy, suggesting that also visual feedback could provide precise information related to the approaching and starting phase of the grasping. In addition, motor memory of fingers position could help subjects in maintaining the same amount of grasping force in absence of haptic feedback. The rate of completed, dropped or broken cubes in the two conditions for the two kinds of cubes are presented in Fig. 13. Though no significant difference was obtained between V and CV conditions, Broken Cube Ratio and Completion Ratio was slightly higher for the V, while dropped ratio was slightly higher for the CV (Completion Ratio V: 73.7, CV: 73.2 percent, Dropped Ratio

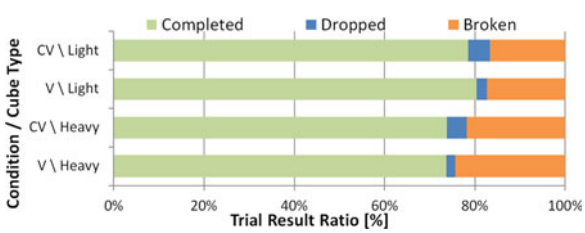

Fig. 13. Average completed ratio of each trial divided between condition (V and CV) and cube type (Light and Heavy).

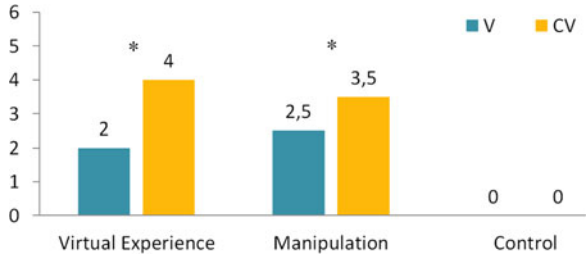

Fig. 14. Responses to the questionnaire for the V and CV conditions, characterized by median value over subjects and question groups.

V: 2.0, CV: 4.4 percent, Broken Ratio V: 24.3, CV: 22.4 percent). Such tiny difference might suggest that the addition of cutaneous feedback improved precision in controlling the force below the breaking force threshold, whereas no improvement was measured for the Dropped Ratio since no information about the slip condition could be rendered by the haptic devices.

With regards to the evaluation questionnaire responses, an analysis of questions aggregated in the three groups (Control, Manipulation and Virtual Experience), is shown in Fig. 14. We conducted a non parametric test (Wilconox Sum Rank Test) on the median value extracted for each group and compared the two conditions, showing a p-value $p < 0.05$ (indicated in Fig. 14 with a star). All subjects answered consistently to the Control questions group with no differences between conditions (average value equal to zero for both V and CV). The analysis of the responses to the Virtual Experience questions group shows that introduction of haptic feedback led users to report higher scores for the CV condition, and in particular the feeling of moving a real object (Q1 and Q2 questions) was significantly higher for the CV condition. This result is likely due to the congruent multisensory feedback and supports the consistency of the cutaneous feedback presented to the subjects. Regarding the Manipulation questions group, the median responses to each question are shown in Fig. 15. Average responses are generally higher for the CV condition, with responses to question Q5 statistically significant in the CV than in the V condition. In addition, significantly higher responses of questions Q13 and Q14 show that cutaneous feedback enhanced control of the applied force and perception of the different physical characteristics of the manipulated objects, supporting the informative role of cutaneous feedback in the manipulation task.

5 Lift-and-Hold Experiment under Controlled Manipulation Conditions

The second manipulation experiment was performed in VR under controlled manipulation condition, in order to better investigate how information rendered by the proposed

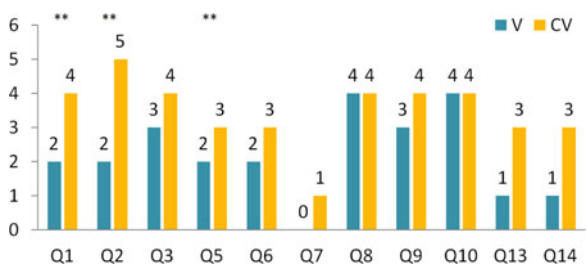

Fig. 15. Responses (median values) to the questionnaire for the V and CV conditions.

TABLE 2
Questionnaire Proposed to the Subjects After the V and CV Experimental Conditions

Question ID	Item	Evaluation Statement
Q1	VIRTUAL EXP	I felt as I was lifting a real object
Q2	VIRTUAL EXP	My interaction with the environment was natural
Q3	VIRTUAL EXP	My experience in the virtual environment was consistent with my real-world experience
Q4	CONTROL	I felt as the starting and the end points changed during the performed task
Q5	MANIPULATION	I perceived when the cubes were slipping
Q6	MANIPULATION	When I perceived the cube was slipping, I was able to recover a stable grasp
Q7	MANIPULATION	It seemed as the cubes had different weights
Q8	MANIPULATION	I perceived that the grasp was stable
Q9	MANIPULATION	I was able to evaluate the force I was applying
Q10	MANIPULATION	I felt I was able to control the applied force
Q11	CONTROL	It seemed as the gravity changed during the interaction in the virtual environment
Q12	CONTROL	I felt the cubes changed their dimensions
Q13	MANIPULATION	I perceived that the black cube was heavier than the grey one
Q14	MANIPULATION	I perceived that the cubes had different resistance

haptic devices was informative and useful during manipulation. For this purpose a simple lift-and-hold task was presented with the addition of a virtual prismatic guide along the vertical axis, similarly to a peg-extraction task. With respect to the pick-and-place experiment, the lift-and-hold task introduced a stationary phase (the final holding phase) where subjects could stabilize the grasping by better focusing on the sensory feedback. Furthermore, the virtual prismatic guide introduced additional physical constraints harder to be perceived by visual feedback only.

5.1 Procedure and Methods

Ten subjects (age 25-31, two female) were enrolled to the experiment, providing written consent to participate. All were right handed and did not present any dysfunction of the fingers. The experimental setup was analogous to the pick-and-place experiment described in Section 4. The virtual scene presented a virtual cube in two dimensional perspective placed in front of the subject as shown in Fig. 16. The cube was constrained by a virtual vertical prismatic guide, graphically represented as a vertical line, constraining all degrees of freedom of the cube, except the vertical translation.

Differently from the pick-and-place experiment, subjects were asked to grasp the virtual cube, to lift it slowly above a 10 cm height threshold, to hold it for 5 seconds, and then to drop it. The height threshold was represented by an horizontal line in the VR scene (Fig. 16). Moreover no upper limit to the virtual interaction forces was set (i.e., breaking of the cube); instead, subjects were expressly asked to perform the lift-and-hold task by keeping virtual interaction forces at the minimum. Subjects had no time constraint in performing the lift phase. They were also informed to hold the cube with a given orientation of the hand, both during grasp and the vertical lift. The minimum required grasping force for lifting the cube was 0.51 N.

As outcome measures, both grasping force (proportional to distance between fingers) and constraint force generated by the virtual prismatic guide (proportional to the position drift on the horizontal plane during the vertical lift) were recorded during the holding phase. The prismatic constraint force was then divided into its tangential and normal components for further evaluation.

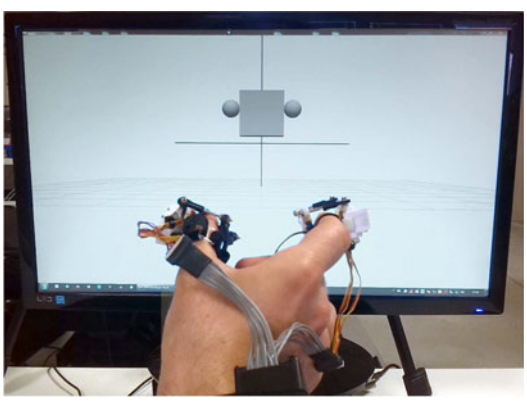

Fig. 16. Experimental setup of the lift-and-hold experiment. Orientation of the hand was held constant during the task. Vertical line in the VR represents the virtual prismatic guide; horizontal line represents the height threshold the cube had to be lifted above.

5.2 Results and Discussion

Results obtained from the lift-and-hold experiment show significantly lower interaction forces in the CV condition than in the V one. Interaction forces of the holding phase (cube above the height threshold) averaged over subjects and trials are shown in Fig. 17.

More in details forces were significantly lower in the CV than in the V for the Grasping Force (Mean V: 1.17 N CV: 0.8 N, $p < 0.015$), for the Prismatic Force (Normal direction) (Mean V: 0.84 N CV: 0.45 N, $p < 0.019$) and for the Prismatic Force (Tangential direction) (Mean V: 1.52 CV: 1.04,

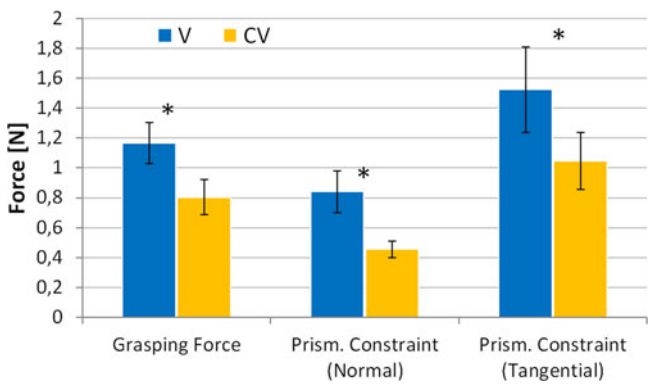

Fig. 17. Interaction forces averaged for all the subjects in the V and CV conditions divided between grasping and prismatic constraint.

$p < 0.033$). Results show that the cutaneous feedback provided consistent information of the virtual physical interaction, allowing subjects to reduce the average interaction forces as required by the proposed task.

Regarding forces generated by the prismatic constraint, it was expected that, by means of cutaneous feedback, subjects could be guided along the vertical direction of lift, whereas with visual feedback only no information of the prismatic constraint was provided, and the following of the vertical trajectory was delegated to proprioception alone. The prismatic constraint was perceived on the direction normal to fingerpads as a differential normal force between index and thumb fingers, and on the distal direction as a tangential stretch of the fingerpads. Results show a similar absolute difference between the V and CV for both Tangential and Normal Prismatic Force (Normal: 0.39 N, Tangential: 0.47 N), although, considering the relative difference, the addition of cutaneous feedback reduced approximately by half the Normal Prismatic Force (V: 0.84 N, CV: 0.45 N). This suggests the prismatic constraint was better perceived on the normal direction, and this might be due to the differential characteristic between index and thumb of the prismatic constraint: subjects were more accurate in balancing the same amount of force between the two fingers than in perceiving an absolute null tangential deformation.

Regarding the grasping force, results show the force in the CV was significantly lower than the V, and with respect to the pick-and-place manipulation experiment, it is evident a higher difference between the V and CV condition. This can be explained by the structure of the proposed task: the lift-and-hold task allowed subjects to focus more on the perceived feedback rather than on dynamic motor actions. Also it induced a slower execution of the task, whereas in the pick-and-place experiment, although no time constraint was provided, subjects tended to move quickly to the target position, probably with the involuntary purpose of reducing the time the cube was lift and thus the chances of dropping the object.

6 Conclusion

A novel wearable haptic device with three DoF for rendering contact forces at the fingerpad has been developed. The main novelty consists in the three-RSR asymmetric rigid parallel kinematics, minimizing the encumbrance with the hand workspace and reducing the mechanical interference with other fingers. An innovative method based on differential kinematics and numerical algorithm has been implemented to solve in real-time the inverse kinematics problem and to control the displacement of the tactor. The device is designed to render constant to low frequency deformation of the fingerpad in three DoF, combining light weight with relatively high output forces. Two prototypes of the device have been manufactured by rapid prototyping to fit the index and thumb fingers; kinematics validation and calibration of the devices have been performed by means of an optical tracking system and a three DoF force sensor. Three experiments regarding discrimination of directional cues and manipulation of virtual objects have been performed to investigate the effectiveness of the cutaneous feedback provided by the proposed devices. The first experiment involved discrimination of radial stretch of the fingerpad among eight different directions. The test was performed by five subjects in stick and slip conditions, and showed good discrimination accuracy with a statistically significant difference in favor of the stick condition. The second experiment involved free manipulation of virtual objects with different simulated mass and breaking threshold. Nineteen subjects performed a pick and place task with the instruction to not break or drop the virtual cubes. The test has been performed with or without cutaneous feedback, demonstrating lower forces in manipulating the objects when haptic feedback is presented, with a low, yet significant, decrease of the interaction forces in the CV for the cubes with higher mass. The third experiment with 10 subjects regarded controlled manipulation of a virtual object in a lift-and-hold task, with interaction forces similar to a peg-extraction task due to the addition of a prismatic constraint. The controlled orientation of the hand, and the regulated sequence of the lift-and-hold task, allowed subjects to better focus on the perceived feedback: it resulted in significant and noticeably higher decrease of all interaction forces (generated by grasping and by the prismatic constraint) in the CV condition.

Together with responses to an evaluation questionnaire, overall results suggest the proposed device was capable of rendering consistent and informative cutaneous feedback, enhancing perception of physical characteristics of the virtual environment, and improving performance of the subjects in controlling the exerted forces within the proposed manipulation tasks.

Acknowledgments

This work has been funded from the EU FP7 project n. 601165 WEARHAP. The authors would like to thank Aditya Kapilavai for his contribution to the work.

References

[1] S. Demain, C. D. Metcalf, G. V. Merrett, D. Zheng, and S. Cunningham, "A narrative review on haptic devices: Relating the physiology and psychophysical properties of the hand to devices for rehabilitation in central nervous system disorders," *Disability Rehabil.: Assistive Technol.*, vol. 8, no. 3, pp. 181–189, 2013.

[2] G. Westling and R. S. Johansson, "Responses in glabrous skin mechanoreceptors during precision grip in humans," *Exp. Brain Res.*, vol. 66, no. 1, pp. 128–140, 1987.

[3] G. Jansson and L. Monaci, "Identification of real objects under conditions similar to those in haptic displays: Providing spatially distributed information at the contact areas is more important than increasing the number of areas," *Virtual Reality*, vol. 9, no. 4, pp. 243–249, 2006.

[4] A. Frisoli, M. Solazzi, F. Salsedo, and M. Bergamasco, "A fingertip haptic display for improving curvature discrimination," *Presence*, vol. 17, no. 6, pp. 550–561, 2008.

[5] F. Chinello, M. Malvezzi, C. Pacchierotti, and D. Prattichizzo, "A three DoFs wearable tactile display for exploration and manipulation of virtual objects," in *Proc. IEEE Haptics Symp.*, 2012, pp. 71–76.

[6] M. W. Wijntjes, A. Sato, V. Hayward, and A. M. Kappers, "Local surface orientation dominates haptic curvature discrimination," *IEEE Trans. Haptics*, vol. 2, no. 2, pp. 94–102, Apr.–Jun. 2009.

[7] A. Frisoli, M. Solazzi, M. Reiner, and M. Bergamasco, "The contribution of cutaneous and kinesthetic sensory modalities in haptic perception of orientation," *Brain Res. Bulletin*, vol. 85, no. 5, pp. 260–266, 2011.

[8] D. Prattichizzo, C. Pacchierotti, and G. Rosati, "Cutaneous force feedback as a sensory subtraction technique in haptics," *IEEE Trans. Haptics*, vol. 5, no. 4, pp. 289–300, Oct.–Dec. 2012.

[9] A. M. Okamura, "Methods for haptic feedback in teleoperated robot-assisted surgery," *Ind. Robot: Int. J.*, vol. 31, no. 6, pp. 499–508, 2004.

[10] C. Pacchierotti, A. Tirmizi, and D. Prattichizzo, "Improving transparency in teleoperation by means of cutaneous tactile force feedback," *ACM Trans. Appl. Perception*, vol. 11, no. 1, 2014, Art. no. 4.
[11] V. Hayward, "Is there a 'plenhaptic' function?" *Philosoph. Trans. Royal Soc. B*, vol. 366, no. 1581, pp. 3115–3122, 2011.
[12] S. L. Norman, A. J. Doxon, B. T. Gleeson, and W. R. Provancher, "Planar hand motion guidance using fingertip skin-stretch feedback," *IEEE Trans. Haptics*, vol. 7, no. 2, pp. 121–130, Apr.–Jun. 2014.
[13] W. R. Provancher, M. R. Cutkosky, K. J. Kuchenbecker, and G. Niemeyer, "Contact location display for haptic perception of curvature and object motion," *Int. J. Robot. Res.*, vol. 24, no. 9, pp. 691–702, 2005.
[14] D. Tsetserukou, S. Hosokawa, and K. Terashima, "LinkTouch: A wearable haptic device with five-bar linkage mechanism for presentation of two-DOF force feedback at the fingerpad," in *Proc. IEEE Haptics Symp.*, 2014, pp. 307–312.
[15] G. Cini, A. Frisoli, S. Marcheschi, F. Salsedo, and M. Bergamasco, "A novel fingertip haptic device for display of local contact geometry," in *Proc. IEEE 1st Joint Eurohaptics Conf., Symp. Haptic Interfaces Virtual Environ. Teleoperator Syst. World Haptics*, 2005, pp. 602–605.
[16] M. Solazzi, A. Frisoli, F. Salsedo, and M. Bergamasco, "A fingertip haptic display for improving local perception of shape cues," in *Proc. IEEE 2nd Joint EuroHaptics Conf., Symp. Haptic Interfaces Virtual Environ. Teleoperator Syst. World Haptics*, 2007, pp. 409–414.
[17] N. Nishimura, D. Leonardis, M. Solazzi, A. Frisoli, and H. Kajimoto, "[D08] wearable encounter-type haptic device with 2-DoF motion and vibration for presentation of friction," in *Proc. IEEE Haptics Symp.*, 2014, pp. 1–1.
[18] D. Prattichizzo, F. Chinello, C. Pacchierotti, and M. Malvezzi, "Towards wearability in fingertip haptics: A 3-DoF wearable device for cutaneous force feedback," *IEEE Trans. Haptics*, vol. 6, no. 4, pp. 506–516, Oct.–Dec. 2013.
[19] Z. F. Quek, S. B. Schorr, I. Nisky, W. R. Provancher, and A. M. Okamura, "Sensory substitution using 3-degree-of-freedom tangential and normal skin deformation feedback," in *Proc. IEEE Haptics Symp.*, 2014, pp. 27–33.
[20] B. T. Gleeson, S. K. Horschel, and W. R. Provancher, "Design of a fingertip-mounted tactile display with tangential skin displacement feedback," *IEEE Trans. Haptics*, vol. 3, no. 4, pp. 297–301, Oct.–Dec. 2010.
[21] W. R. Provancher and N. D. Sylvester, "Fingerpad skin stretch increases the perception of virtual friction," *IEEE Trans. Haptics*, vol. 2, no. 4, pp. 212–223, Oct.–Dec. 2009.
[22] V. G. Macefield, C. Häger-Ross, and R. S. Johansson, "Control of grip force during restraint of an object held between finger and thumb: Responses of cutaneous afferents from the digits," *Exp. Brain Res.*, vol. 108, no. 1, pp. 155–171, 1996.
[23] D. Leonardis, M. Solazzi, I. Bortone, and A. Frisoli, "A wearable fingertip haptic device with 3 DoF asymmetric 3-RSR kinematics," in *Proc. IEEE World Haptics Conf.*, 2015, pp. 388–393.
[24] L.-W. Tsai, *Robot Analysis: The Mechanics of Serial and Parallel Manipulators*. Hoboken, NJ, USA: Wiley, 1999.
[25] R. S. Ball, *A Treatise on the Theory of Screws*. Cambridge, U.K.: Cambridge Univ. Press, 1998.
[26] R. Hertz and P. Hughes, "Kinematic analysis of a genaral double-tripod parallel manipulator," *Mechanism Mach. Theory*, vol. 33, no. 6, pp. 683–696, 1998.
[27] J. Kim and F. Park, "Direct kinematic analysis of 3-RS parallel mechanisms," *Mechanism Mach. Theory*, vol. 36, no. 10, pp. 1121–1134, 2001.
[28] R. Di Gregorio, "Inverse position analysis, workspace determination and position synthesis of parallel manipulators with 3-RSR topology," *Robotica*, vol. 21, no. 6, pp. 627–632, Dec. 2003. [Online]. Available: http://dx.doi.org/10.1017/S0263574703005174
[29] B. T. Gleeson, S. K. Horschel, and W. R. Provancher, "Perception of direction for applied tangential skin displacement: Effects of speed, displacement, and repetition," *IEEE Trans. Haptics*, vol. 3, no. 3, pp. 177–188, Jul.–Sep. 2010.
[30] K. J. Cole and J. H. Abbs, "Grip force adjustments evoked by load force perturbations of a grasped object," *J. Neurophysiology*, vol. 60, no. 4, pp. 1513–1522, 1988.
[31] M. Bergamasco, C. A. Avizzano, A. Frisoli, E. Ruffaldi, and S. Marcheschi, "Design and validation of a complete haptic system for manipulative tasks," *Adv. Robot.*, vol. 20, no. 3, pp. 367–389, 2006.
[32] M. Carrozzino, F. Tecchia, S. Bacinelli, C. Cappelletti, and M. Bergamasco, "Lowering the development time of multimodal interactive application: The real-life experience of the XVR project," in *Proc. ACM SIGCHI Int. Conf. Advances Comput. Entertainment Technol.*, 2005, pp. 270–273.
[33] B. G. Witmer and M. J. Singer, "Measuring presence in virtual environments: A presence questionnaire," *Presence: Teleoperators Virtual Environ.*, vol. 7, no. 3, pp. 225–240, 1998.
[34] Q. Wang and V. Hayward, "In vivo biomechanics of the fingerpad skin under local tangential traction," *J. Biomechanics*, vol. 40, no. 4, pp. 851–860, 2007.

Daniele Leonardis received the BS and MS degrees in automation engineering from the Politecnico of Bari, Italy, in 2007 and 2009, respectively, and the PhD degree in innovative technologies from PERCRO Laboratory, Scuola Superiore Sant'Anna, Pisa, Italy, in 2015. His research interests deal with haptic feedback applied to telepresence and virtual embodiment, and bio-signals (BCI and EMG) for controlling robotic devices. He is a member of the IEEE.

Massimiliano Solazzi received the PhD degree from the Scuola Superiore Sant'Anna, Pisa, Italy, in 2010. He is an assistant professor of applied mechanics with the Scuola Superiore Sant'Anna, Pisa, Italy. He carries out his research in the Percro Laboratory—TeCIP. His research interests concerns the design of robotic interfaces for virtual reality, teleoperation and rehabilitations, and the psychophysical validation of HMI. He is a member of the IEEE.

Ilaria Bortone received the BS and MS degrees in biomedical engineering from the University of Pisa, Italy, in 2009 and 2011, respectively. She is currently working toward the PhD degree in emerging digital technologies in the PERCRO Laboratory, Scuola Superiore Sant'Anna, Pisa, Italy. Her research interests deal with biomechanics and neurorehabilitation in virtual reality environments. She is a student member of the IEEE.

Antonio Frisoli received the MSc degree in mechanical engineering from Scuola Superiore Sant'Anna, Italy, in 1988, and the PhD degree with honors in industrial and information engineering from Scuola Superiore Sant'Anna, Italy, in 2002. He is an associate professor of mechanical engineering with Scuola Superiore Sant'Anna, where he is currently a head of the Human-Robot Interaction area at the PERCRO Laboratory—TeCIP and former chair of the IEEE Technical Committee on Haptics. His research interests concern the design and control of haptic devices and robotic systems, rehabilitation robotics, advanced HRI, and kinematics. He is a member of the IEEE.